Electrochemical kinetics of $Na_2Ti_3O_7$ as anode material for lithium-ion batteries

Haojie Zhu [1], Ke Yang [1], Hua Lan, Shangshu Qian, Haoxiang Yu, Lei Yan, Nengbing Long, Miao Shui, Jie Shu *

Faculty of Materials Science and Chemical Engineering, Ningbo University, Ningbo 315211, Zhejiang Province, People's Republic of China

A B S T R A C T

In this work, $Na_2Ti_3O_7$ is fabricated as lithium storage material *via* one-step solid state reaction. Worked as anode material, $Na_2Ti_3O_7$ delivers a stable electrochemical performance with good lithium storage capability. Structural analyses show that $Na_2Ti_3O_7$ anode experiences slight volume change during electrochemical lithiation/delithiation process. Moreover, the reversibility of structural evolution is further demonstrated by *in-situ* X-ray diffraction technique. All these evidences prove the cycling stability of $Na_2Ti_3O_7$ as lithium storage material. Besides, the kinetic properties of the Li^+ ion storage in $Na_2Ti_3O_7$ are systematically investigated. The observed results reveal that $Na_2Ti_3O_7$ delivers the lithium ions diffusion coefficient in the range of 10^{-14}–10^{-12} cm^2 s^{-1} during the discharge process and 10^{-15}–10^{-12} cm^2 s^{-1} during the recharge process. It suggests that $Na_2Ti_3O_7$ has good lithiation/delithiation kinetics in rechargeable batteries.

© 2017 Elsevier B.V. All rights reserved.

1. Introduction

Energy is not only the most important basis of the progress of human society, but also one of the basic driving forces of economic development. However, the short of fossil energy arouses serious energy crisis all over the world, which drives the material scientists to develop new energy sources. As a novel energy storage and conversion system, rechargeable lithium-ion batteries have been widely used in electronic equipments in the past twenty years. It becomes the main power of the portable electronic devices due to its considerable energy density, long cycle calendar life and low self-discharge [1–9]. Graphite is a traditional anode material for commercial lithium-ion batteries. However, it suffers from safety issues due to low operating potential (0.1 V *vs.* Li^+/Li). Thus, alternative anode materials are developed to replace graphite. Recent years, titanium-based oxides have been put forward to be the distinguished substitutions because of their high working potential and stability electrochemical property [10–12].

Among titanium-based oxides, $Na_2Ti_3O_7$ has been used as a possible anode material for rechargeable batteries since its ability to store sodium was first found in 2011 [13]. Since the discovery of its electrochemical activity in 2011, $Na_2Ti_3O_7$ has attracted much attention because of the great potential as anode material [14–16]. It is found that $Na_2Ti_3O_7$ can store two moles of sodium ions per formula to form $Na_4Ti_3O_7$ in

sodium-ion batteries [17]. However, $Na_2Ti_3O_7$ suffers from poor electrochemical activity. Hence, various methods have been used to improve its sodium storage ability. Recently, carbon-encapsulated $Na_2Ti_3O_7$ particles have been testified successfully in increasing the electrochemical property of the anode material [18]. Employing the spray-drying method, Li et al. prepared micro-spherical $Na_2Ti_3O_7$ which has high sodium storage capacity and stable cycle performance [19,20]. As well-known, the alkali titanium, having the general formula of $A_2Ti_nO_{2n+1}$ (A = alkali metals; $2 \le n \le 9$), can also show high Li^+ ion conductivity and storage capability. Preliminary investigation reveals that $Na_2Ti_3O_7$ anode material has high and flat working platform (about 1.6 V) in lithium-ion batteries [21]. However, detailed electrochemical research and lithium storage behaviors have not been reported.

In this article, well-crystallized $Na_2Ti_3O_7$ is synthesized by a solid-state method and its Li storage performance is evaluated. It is found that $Na_2Ti_3O_7$ has good structural stability as anode material for lithium-ion batteries. No obvious structural changes can be observed from the *in-situ* XRD observation. In addition, the lithium ions diffusion coefficient in $Na_2Ti_3O_7$ is also studied by cyclic voltammetry (CV) and electrochemical impedance spectroscopy (EIS) methods. The observed data show that $Na_2Ti_3O_7$ has good electrochemical kinetics in lithium-ion batteries.

2. Experimental

2.1. Synthesis of $Na_2Ti_3O_7$

$Na_2Ti_3O_7$ was synthesized by a traditional solid-state reaction method. All the chemical reagents were analytical grade in the experiment.
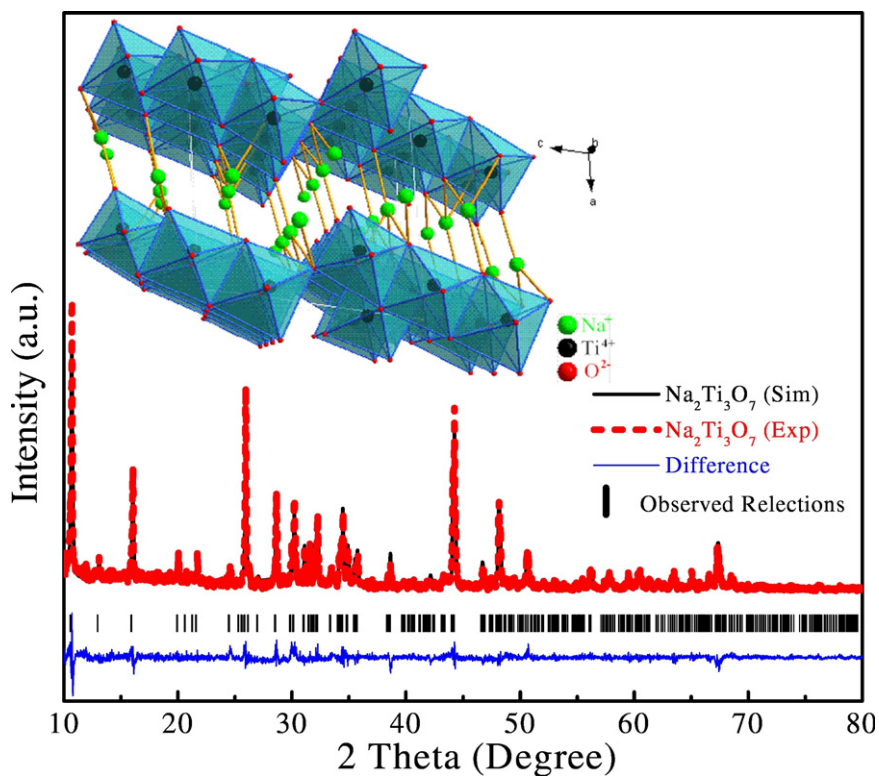
Fig. 1. XRD pattern of $Na_2Ti_3O_7$ powder.

TiO_2 (Aladdin Chemical, 99.8%) and anhydrous Na_2CO_3 (Aladdin Chemical, 99.0%) were used as starting materials. Then the precursor powders were mixed with ethanol and ground in the planetary ball mill for 12 h. The resultant specimen was transferred into a muffle furnace and heat-treated at 800 °C for 10 h in air atmosphere. After cooling down to room temperature naturally, the final product was formed.
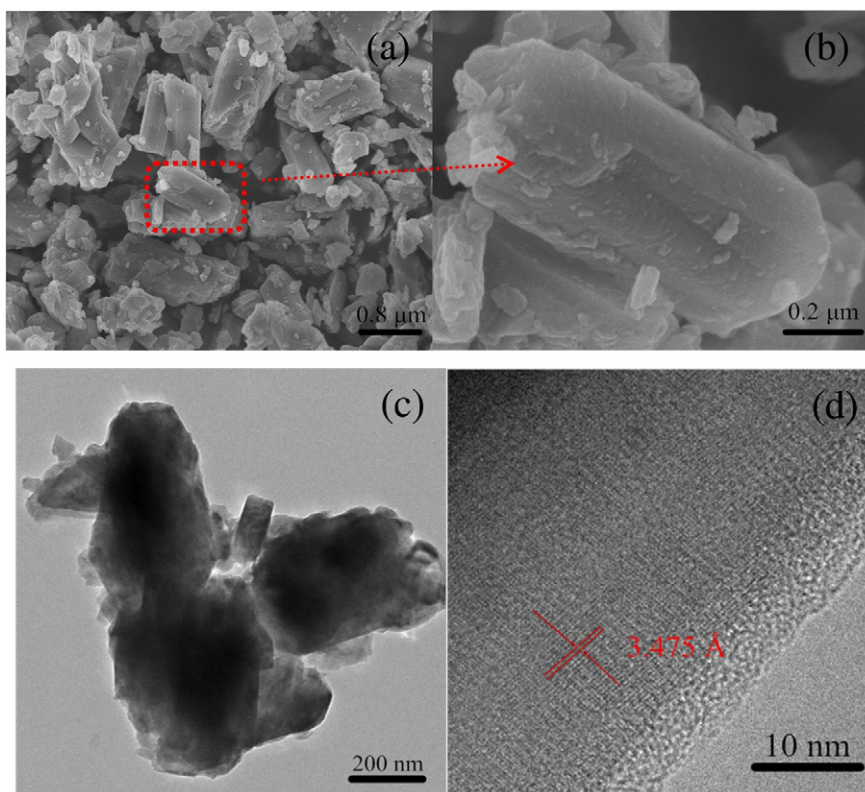

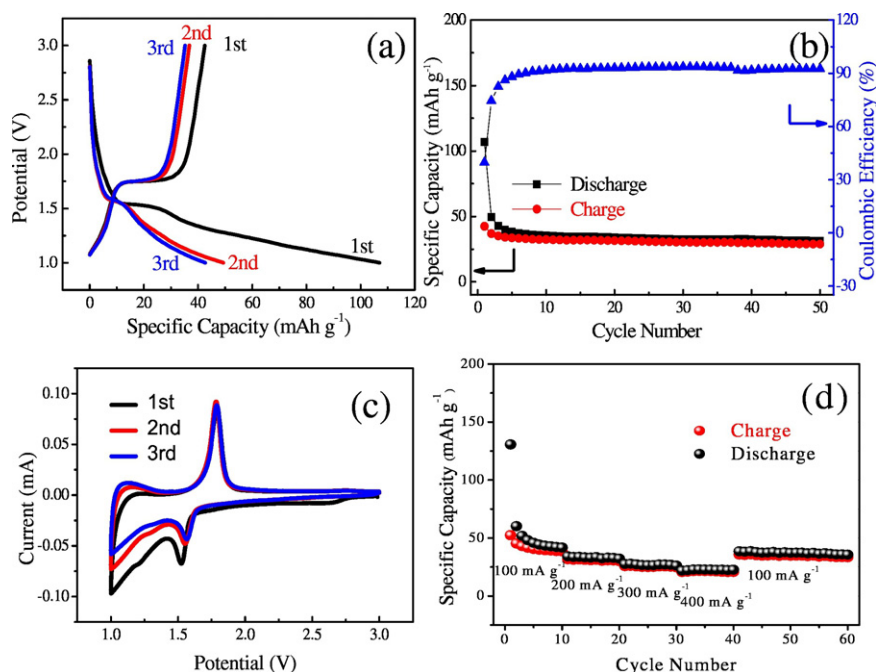**Fig. 2.** (a, b) SEM and (c, d) TEM images of $Na_2Ti_3O_7$ powder.

Fig. 3. (a) The first three charge-discharge curves (100 mA g^{-1}), (b) cyclic performance and Coulombic efficiency, (c) the initial three CVs, and (d) the rate performance for Na$_2$Ti$_3$O$_7$.

2.2. Materials characterization

The phase purity and crystal structure of the obtained powders were characterized by powder X-ray diffraction using a Bruker D8 diffractometer (Cu-Kα radiation, λ = 1.5406 Å). The particle morphology was observed by Hitachi SU70 scanning electron microscopy (SEM). Crystal symmetry was in addition studied by means of JEOL JEM-2010 high resolution transmission electron microscope (HRTEM) and selected area electron diffraction (SAED).

2.3. Electrochemical tests

For the electrochemical study, the working electrode was prepared by pasting a homogeneous slurry containing 70 wt% Na$_2$Ti$_3$O$_7$ active material, 20 wt% carbon black conductive additive, and 10 wt% polyvinyl fluoride binder dispersed in N-methyl-2-pyrrolidone (Mclean) on a Cu foil and subsequently dried in vacuum oven at 80 °C for 12 h. Then, the as-prepared film was cut into disks with a diameter of 15 mm. The CR2032 typed coin cells were assembled in an argon-filled glove box with the as-prepared film as the working electrode, Li metal foil as the counter electrode, glass fiber as the separator and 1 mol L^{-1} LiPF$_6$ dissolved in a mixture of ethylene carbonate and dimethyl carbonate (1:1 in volume) as the electrolyte.

The charge-discharge properties of sample cells were measured at a current density of 100 mA g^{-1} between 1.0 and 3.0 V by multichannel LANHE battery test system at room temperature (25 °C). Cyclic voltammetry (CV) was carried out between 1.0 and 3.0 V with a scan rate of 0.1 mV s^{-1} by CHI 1000B electrochemical workstation at room temperature. Electrochemical impedance spectroscopy (EIS) analysis was carried out by CHI 660D electrochemical workstation with the frequency range of 10^{-2}–10^5 Hz.

3. Results and discussion

Fig. 1 shows the refinement XRD pattern of the Na$_2$Ti$_3$O$_7$ sample. It can be found that the observed reflections are well consistent with standard Bragg positions of Na$_2$Ti$_3$O$_7$ (JCPDS card No. 31-1329).

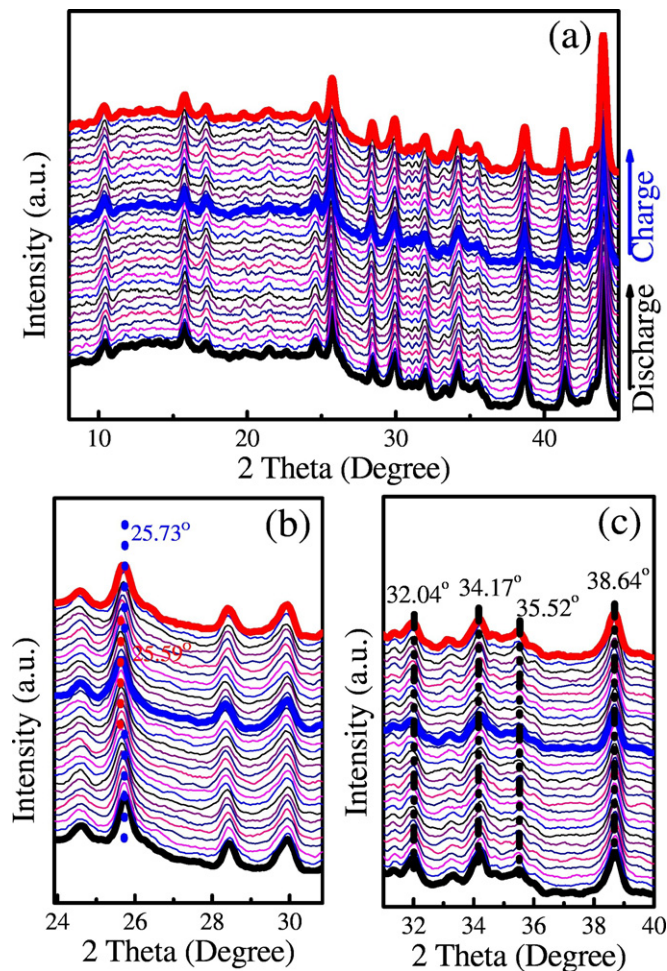**Fig. 4.** *In-situ* XRD patterns of Na$_2$Ti$_3$O$_7$ electrode during the initial charge-discharge process between 1.0 and 3.0 V. (a) The whole range, (b) range from 24 to 31°, (c) range from 31 to 40°.

Furthermore, the refined cell parameters (a = 8.5634(3) Å, b = 3.7997(1) Å, c = 9.1260(3) Å, α = 90.000(0)° and β = 101.593(2)°) are also obtained from XRD Rietveld refinement, suggesting the successful formation of high purity $Na_2Ti_3O_7$ via solid state reaction. In addition, Fig. 1 also displays the crystal structure of $Na_2Ti_3O_7$, in which each TiO_6 octahedron exhibits a shared-vertex with other two edge-shared octahedra in a crystallographic shear structure. This structural characteristic belongs to a typical Wadsley-Roth class. Among TiO_6 sheets, Na atoms distribute in two different crystallographic coordinations. In the three-dimensional tunnels built from TiO_6 octahedra, there are lots of empty octahedral and tetrahedral sites available for lithium ions insertion.

To explore the morphology of the prepared sample, SEM and TEM analyses are carried out. Fig. 2a shows the surface morphology of the $Na_2Ti_3O_7$ powder, which consists of irregular particles with the average size of 0.4–1.5 μm. With a close observation (Fig. 2b), it is known that the surface of particles is decorated with small primary nanoparticles in the size of 20–40 nm. Fig. 2c and d present the TEM and SEM images of the as-prepared $Na_2Ti_3O_7$ powder. Irregular particles with size of 300 nm in width and 1.0 μm in length are observed. Fig. 2d clearly shows that the powder material has a lattice fringe of 3.475 Å, which corresponds to the featured (011) reflection of $Na_2Ti_3O_7$.

The charge-discharge curves and corresponding cycling property of $Na_2Ti_3O_7$ are shown in Fig. 3a–b. Here, $Na_2Ti_3O_7$ presents the initial three charge-discharge curves collected at a current density of 100 mA g^{-1} between 1.0 and 3.0 V (Fig. 3a). It can be clearly observed that $Na_2Ti_3O_7$ shows one pair of charge/discharge plateaus at 1.75/1.50 V and one lithiation slope between 1.0 and 1.5 V. With a careful observation in Fig. 3b, it is known that $Na_2Ti_3O_7$ delivers the initial charge-

discharge capacities of 42.5/107.0 mAh g^{-1} with its first Columbic efficiency of 41.9%. After 50 cycles, it can retain a charge capacity retention of 68% owing to the reversible lithiation-delithiation behaviors in the $Na_2Ti_3O_7$ host structure. Fig. 3c presents the CVs of $Na_2Ti_3O_7$ in the potential range of 1.0–3.0 V. During the first scan, a sharp reduction peak can be observed at 1.52 V, with a corresponding oxidation peak locating at 1.79 V. Upon subsequent scans, the reduction peak shifts to higher operating potentials. For comparison, almost no change can be detected for the oxidation peak. It indicates that the redox polarization gradually decreases with repeated cycles, which is beneficial to achieve good calendar life. Fig. 3d shows the rate performance of $Na_2Ti_3O_7$ sample recorded at different current densities. It delivers the average charge-discharge capacities of 31.5/33.9, 26.2/27.5, and 21.7/23.0 mAh g^{-1} at the current densities of 200, 300 and 400 mA g^{-1}, respectively. It suggests that lithium ions can transfer rapidly in the structure of $Na_2Ti_3O_7$.

In order to study the structural evolution of $Na_2Ti_3O_7$ material, in-situ XRD measurements are taken in the potential range of 1.0–3.0 V as displayed in Fig. 4. For the first XRD pattern, five featured peaks centered at 25.73°, 32.04°, 34.17°, 35.52° and 38.64° are the same as the featured planes of $Na_2Ti_3O_7$ (JCPDS card No. 31-1329). With the gradual insertion of lithium ions in the structure, the featured peak at 25.73° shifts towards to lower angles. It is clear that this featured peak of $Na_2Ti_3O_7$ moves to 25.59° after a discharge process to 1.0 V. At the same time, other featured peaks still maintain their Bragg positions during lithiation process. Upon a recharge process to 3.0 V, all the reflections can return to the pristine positions. The transformation of featured peaks in the initial cycle can also be demonstrated by the patterns of relative intensity versus 2θ as shown in Fig. S1 (Supplementary materials). All these phenomena suggest that $Na_2Ti_3O_7$ sample has high

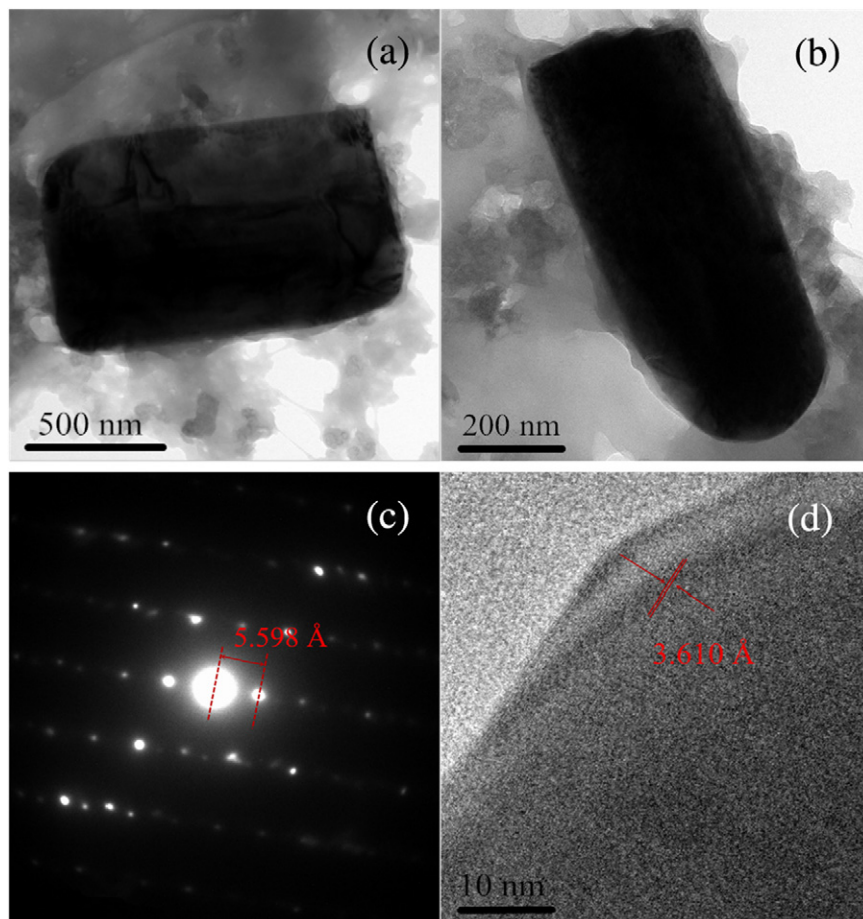**Fig. 5.** (a, b) TEM, (c) SAED and (d) HRTEM images of $Na_2Ti_3O_7$ after discharging to 0.0 V.

structural stability and electrochemical reversibility during lithiation-delithiation process.

The TEM, HRTEM and SAED images of $Na_2Ti_3O_7$ electrode after a discharge process to 0.0 V are shown in Fig. 5. In Fig. 5a and b, the particle size of as-prepared $Na_2Ti_3O_7$ is about 400–600 nm in width and 800–1200 nm in length, surrounding with carbon black conductive additive (about 30 nm). It can be found that the structure of $Na_2Ti_3O_7$ particles keep stably after a full lithiation process to 0.0 V. As shown in Fig. 5c, the fringe spacing is 5.598 Å for lithiated $Na_2Ti_3O_7$ in SAED image, corresponding to the (101) featured reflection. Meanwhile, the d-spacing of the (011) plane increases from 3.475 to 3.610 Å after full lithiation in HRTEM images as displayed in Fig. 5d. It means that the insertion of Li^+ ions leads to a slight expansion of the lattice volume, which is in consistent with the structural evolution of lithiated $Li_4Ti_5O_{12}$ [22,23]. After a recharge process to 3.0 V, $Na_2Ti_3O_7$ particles still maintain the host structure as shown in Fig. 6a and b. At the same time, the fringe spacings can be measured to be 5.524 and 3.501 Å in the SAED and HRTEM images (Fig. 6c and d) after a recharge process to 3.0 V, respectively. It shows that the d-spacings of the (101) and (011) planes almost shrink to the pristine values after full delithiation. The results of these structural transformations prove the high structural stability and electrochemical reversibility of $Na_2Ti_3O_7$ as lithium storage anode material.

To study the electrochemical kinetics of $Na_2Ti_3O_7$ during lithiation/delithiation process, Fig. 7a shows the cyclic voltammograms recorded at the scan rates of 0.1, 0.2, 0.5 and 1.0 mV s^{-1} between 1.0 and 3.0 V. It clearly shows a pair of separated redox peaks (1.56/1.81 V) at a scan rate of 0.1 mV s^{-1}. As the scan rate increases, the oxidation peak shifts to higher potentials, while the reduction peak shifts to lower potentials. At the same time, the redox peak current gradually increases. The relationship between peak current and the square root of scan rate is displayed in Fig. 7b, which reveals a standard linear behavior for

lithiation/delithiation process. It tells that lithium ions diffuse in the $Na_2Ti_3O_7$ electrode with a linear semi-infinite behavior. Thus, its lithium ions diffusion coefficient can be received by the following equation [24, 25]:

$$i_p = \left(2.69 \times 10^5\right)n^{3/2}AD_{Li^+}^{1/2}C_{Li^+}\nu^{1/2} \tag{1}$$

Here, i_p is the peak current, n is the charge-transfer number for redox reaction, A is the contact area of the electrode, C_{Li^+} is the concentration of lithium ions in the electrode, and ν is the scan rate (V s^{-1}). As a result, $Na_2Ti_3O_7$ electrode presents the chemical diffusion coefficient of 1.278×10^{-12} cm^2 s^{-1} at the discharge process and 1.095×10^{-12} cm^2 s^{-1} at the recharge process, which is similar with the values of $Li_4Ti_5O_{12}$ [21].

As well-known, EIS is another effective technique to investigate the chemical diffusion coefficient in the solid. Fig. 7c and d show the EIS curves collected during lithiation/delithiation process, which are composed of a depressed semicircle in the high frequency region and an inclined line in the low frequency region. The semicircle in the high frequency region represents the charge-transfer process, while the oblique line in the low frequency region reflects the lithium ions diffusion process in the structure of $Na_2Ti_3O_7$. A corresponding equivalent circuit in Fig. 7c is used to simulate the diffusion kinetics process of lithium ion in $Na_2Ti_3O_7$. Here, the lithium ions diffusion coefficient (D_{Li}) of $Na_2Ti_3O_7$ could be roughly calculated according to the following equation [26–29]:

$$D_{Li} = \frac{R^2T^2}{2A^2n^4F^4C^2\sigma^2} \tag{2}$$

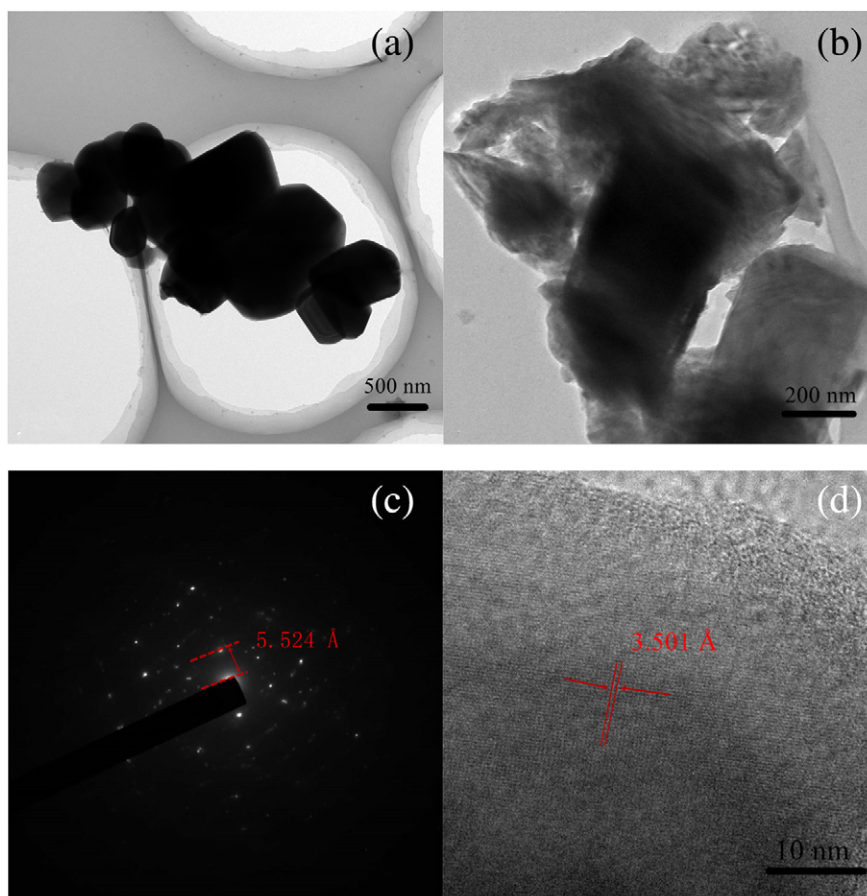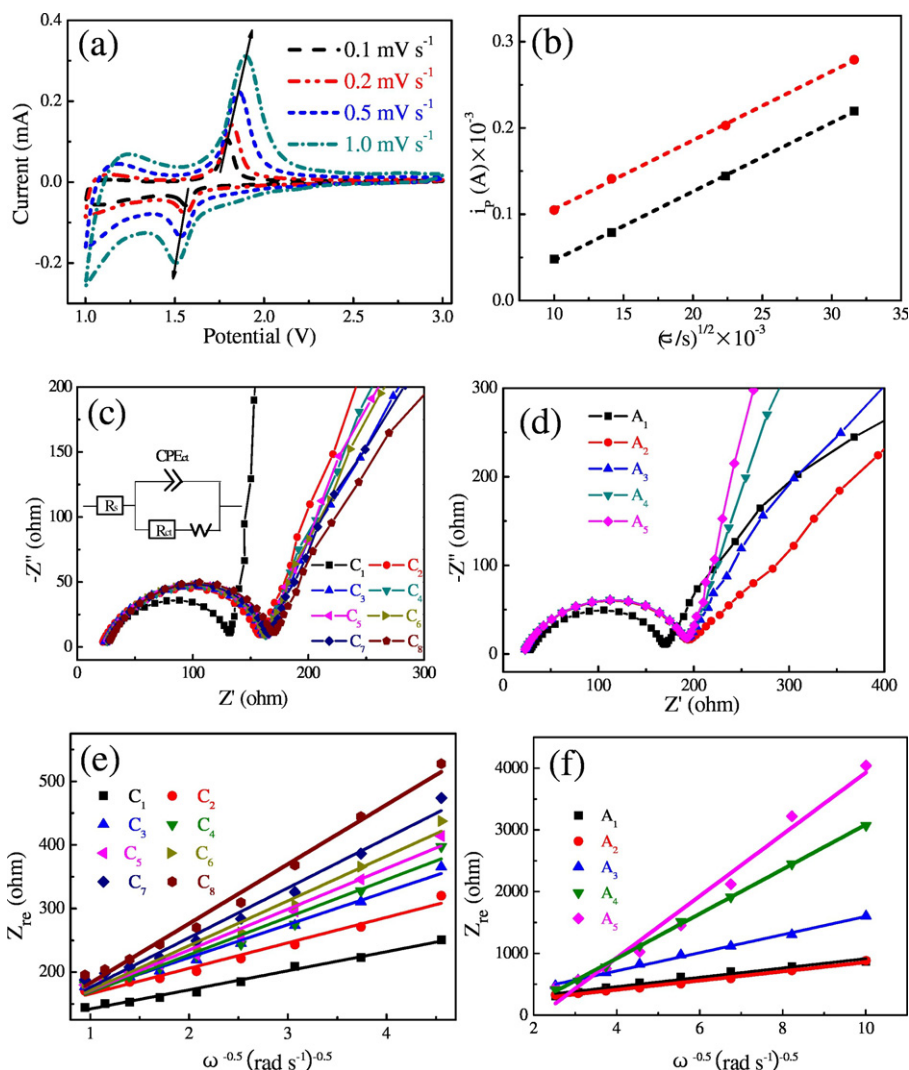**Fig. 6.** (a, b) TEM, (c) SAED and (d) HRTEM images of $Na_2Ti_3O_7$ electrode after recharging to 3.0 V.

Fig. 7. (a, b) Cyclic voltammetry curves of the $Na_2Ti_3O_7$ electrode at different scan rates of 0.1, 0.2, 0.5 and 1.0 mV s^{-1} between 1.0 and 3.0 V; (c, d) the Nyquist plots at different lithiated/delithiated states (C: cathodic process, A: anodic process) for the $Na_2Ti_3O_7$ electrode; (e, f) the plots of the real part of impedance (Z′) for discharge and charge process as a function of the inverse square root of angular frequency ($\omega^{-0.5}$) at different lithiated/delithiated states in the Warburg region.

where the meaning of R is the gas constant (8.314 J mol^{-1} K^{-1}), T is the absolute temperature (298 K), A is the surface area of the electrode (1.77 cm^2), n is the number of electrons transferred in the half-reaction for the redox couple, F is the Faraday constant (96,500 C mol^{-1}), C is the molar concentration of Li$^+$, and σ is the Warburg factor, which has relationship with Z′ based on the following equation [26–29]:

$$Z' = R_e + R_{ct} + \sigma\omega^{-1/2} \tag{3}$$

where R_e is the resistance of electrolyte, R_{ct} is the charge transfer resistance and ω is the angular frequency. σ is obtained from the slope of Z′ vs. $\omega^{-1/2}$ plot as shown in Fig. 7e and f. According to the calculated results presented in Tables 1 and 2, it is obvious that $Na_2Ti_3O_7$ delivers the lithium ions diffusion coefficient in the range of 10^{-14}–10^{-13} cm^2 s^{-1} during the discharge process and shows the value in

the range of 10^{-15}–10^{-13} cm^2 s^{-1} during the recharge process. These calculated data are close to the D_{Li} values from CVs. It suggests that $Na_2Ti_3O_7$ has good electrochemical kinetics in lithium-ion batteries.

4. Conclusions

In summary, $Na_2Ti_3O_7$ is prepared by a traditional solid state reaction. Used as anode material, $Na_2Ti_3O_7$ shows an initial discharge capacity of 107.0 mAh g^{-1}, suggesting the possibility as lithium host material. After repeated cycles, $Na_2Ti_3O_7$ can maintain good capacity retention, suggesting its high structural stability. Furthermore, TEM, HRTEM and SAED images also demonstrate its stable host structure with slight expansion/shrinkage of lattice volume during discharge/charge process. Besides, *in-situ* XRD investigation reveals that $Na_2Ti_3O_7$ has high electrochemical and structural reversibility during lithiation/delithiation

Table 1
The σ values and corresponding lithium diffusion coefficients at different lithiated states during discharge process.

Lithiated state	C_1	C_2	C_3	C_4	C_5	C_6	C_7	C_8
σ/Ω s$^{-0.5}$	30.010	40.104	51.852	59.146	64.223	70.426	78.250	93.530
$D_{Li} \times 10^{-14}$ cm^2 s^{-1}	65.97	36.94	22.10	16.98	14.40	11.98	9.702	6.791

Table 2
The σ values and corresponding lithium diffusion coefficients at different delithiated state during charge process.

Delithiated state	A_1	A_2	A_3	A_4	A_5
σ/Ω s$^{-0.5}$	75.582	74.055	146.769	499.444	360.813
$D_{Li} \times 10^{-15}$ cm^2 s^{-1}	104.0	108.3	27.58	2.382	4.563

process. It concludes that $Na_2Ti_3O_7$ is structurally stable as electrode material for rechargeable lithium-ion batteries.

Acknowledgments

Appendix A. Supplementary data

Supplementary data to this article can be found online at http://dx.doi.org/10.1016/j.jelechem.2017.02.013.

References

[1] C. Liu, F. Li, L.P. Ma, H.M. Cheng, Advanced materials for energy storage, Adv. Energy Mater. 22 (2010) E28–E62.
[2] B. Scrosati, J. Garche, Lithium batteries: status, prospects and future, J. Power Sources 195 (2010) 2419–2430.
[3] N.S. Choi, Z.H. Chen, S.A. Freunberger, X.L. Ji, Y.K. Sun, K. Amine, G. Yushin, L.F. Nazar, J. Cho, P.G. Bruce, Challenges facing lithium batteries and electrical double-layer capacitors, Angew. Chem. Int. Ed. 51 (2012) 9994–10024.
[4] B. Scrosati, J. Hassoun, Y.K. Sun, Lithium-ion batteries. A look into the future, Energy Environ. Sci. 4 (2011) 3287–3295.
[5] Wolfgang H. Meyer, Polymer electrolytes for lithium-ion batteries, Adv. Mater. 10 (1998) 439–448.
[6] X.X. Jiang, K.Q. Wu, L.Y. Shao, M. Shui, X.T. Lin, M.M. Lao, N.B. Long, Y.L. Ren, J. Shu, Lithium storage mechanism in superior high capacity copper nitrate hydrate anode material, J. Power Sources 206 (2012) 218–224.
[7] P. Hu, X.F. Wang, J. Ma, Z.H. Zhang, J.J. He, X.G. Wang, S.Q. Shi, G.L. Cui, L.Q. Chen, $NaV_3(PO_4)_3$/C nanocomposite as novel anode material for Na-ion batteries with high stability, Nano Energy 26 (2016) 382–391.
[8] S. Shi, J. Gao, Y. Liu, Y. Zhao, Q. Wu, W. Ju, C. Ouyang, R. Xiao, Multi-scale computation methods: their applications in lithium-ion battery research and development, Chin. Phys. B 25 (2015) 018212.
[9] J.L. Yue, Y.N. Zhou, S.Q. Shi, Z. Shadike, X.Q. Huang, J. Luo, Z.Z. Yang, H. Li, L. Gu, X.Q. Yang, Z.W. Fu, Discrete Li-occupation versus pseudo-continuous Na-occupation and their relationship with structural change behaviors in $Fe_2(MoO_4)_3$, Sci. Report. 5 (2015) 8810.
[10] J.B. Goodenough, Y. Kim, Lithium intercalation into $ATi(PS_4)_3$ (A = Li, Na, Ag), Electrochem. Commun. 10 (2008) 497–501.
[11] J. Kang, A.K. Rai, S. Kim, E. Choi, I. Yoo, J. Kim, J. Kim, Synthesis of Ti-based electrodes using Ti-salt flocculated sludge and their application in lithium-ion batteries, Mater. Res. Bull. 47 (2012) 2834–2837.
[12] J. Xu, C. Ma, M. Balasubramanian, Y.S. Meng, Understanding $Na_2Ti_3O_7$ as an ultra-low voltage anode material for Na-ion battery, Chem. Commun. 75 (2014) 10901–10904.
[13] D. Pal, R.K. Pal, J.L. Pandey, S.H. Abdi, A.K. Agnihotri, Bulk ac conductivity studies of lithium substituted layered sodium trititanates ($Na_2Ti_3O_7$), J. Mater. Sci. Mater. Electron. 21 (2010) 1181–1185.
[14] W. Wang, C.J. Yu, Z.S. Lin, J.G. Hou, H.M. Zhu, S.Q. Jiao, Microspheric $Na_2Ti_3O_7$ consisting of tiny nanotubes: an anode material for sodium-ion batteries with ultra-fast charge-discharge rates, Nanoscale 5 (2013) 594–599.
[15] A. Rudola, K. Saravanan, C.W. Mason, P. Balaya, $Na_2Ti_3O_7$: an intercalation based anode for sodium-ion battery applications, J. Mater. Chem. A 1 (2013) 2653–2662.
[16] M.M. Doeff, J. Cabana, M. Shirpour, Titanate anodes for sodium ion batteries, J. Inorg. Organomet. Polym. 24 (2014) 5–14.
[17] H. Pan, X. Lu, Y.S. Hu, H. Li, X.Q. Yang, L. Chen, Sodium storage and transport properties in layered $Na_2Ti_3O_7$ for room-temperature sodium-ion batteries, Adv. Energy Mater. 3 (2013) 1186–1194.
[18] Y.P. Zhang, L. Guo, S.H. Yang, Three-dimensional spider-web architecture assembled from $Na_2Ti_3O_7$ nanotubes as a high performance anode for a sodium-ion battery, Chem. Commun. 50 (2014) 14029–14032.
[19] W. Zou, J.W. Li, Q.J. Deng, J. Xue, X.Y. Dai, A.J. Zhou, J.Z. Li, Microspherical $Na_2Ti_3O_7$ prepared by spray-drying method as anode material for sodium-ion battery, Solid State Ionics 262 (2014) 192–196.
[20] W. Zou, Y. Wang, Z.L. Huang, J.Z. Li, Synthesis of $Na_2Ti_3O_7$@MWCNTs anode material by spray-drying method of sol-gel precursor for sodium-ion batteries, Sci. China Chem. 44 (2014) 1347–1353.
[21] G. Rousse, M.E. Arroyo-de Dompable, P. Senguttuvan, A. Ponrouch, J.M. Tarascon, M.R. Palacín, Rationalization of intercalation potential and redox mechanism for $A_2Ti_3O_7$ (A = Li, Na), Chem. Mater. 25 (2013) 4946–4956.
[22] P. Senguttuvan, G. Rousse, V. Seznec, J.M. Tarascon, M.R. Palacín, $Na_2Ti_3O_7$: lowest voltage ever reported oxide insertion electrode for sodium ion batteries, Chem. Mater. 23 (2011) 4109–4111.
[23] J.K. Shin, K.Y. Chung, J.H. Ryu, I.W. Park, D.H. Yoon, Effects of Li/Ti ratios on the electrochemical properties of $Li_4Ti_5O_{12}$ examined by time-resolved X-ray diffraction, Appl. Phys. A Mater. Sci. Process. 107 (2012) 769–775.
[24] S.T. Wang, Y. Yang, W. Quan, Y. Hong, Z.T. Zhang, Z.L. Tang, J. Li, Ti^{3+}-free three-phase $Li_4Ti_5O_{12}$ for high-rate lithium ion batteries: Capacity and conductivity enhancement by phase boundaries, Nano Energy 32 (2017) 294–301.
[25] C. Wang, S. Wang, L.K. Tang, Y.B. He, L. Gan, J. Li, H.D. Du, B.H. Li, Z.Q. Lin, F.Y. Kang, A robust strategy for crafting monodisperse $Li_4Ti_5O_{12}$ nanospheres as superior rate anode for lithium ion batteries, Nano Energy 21 (2016) 133–144.
[26] T.F. Yi, S.Y. Yang, M. Tao, Y. Xie, Y.R. Zhu, R.S. Zhu, Synthesis and application of a novel $Li_4Ti_5O_{12}$ composite as anode material with enhanced fast charge-discharge performance for lithium-ion battery, Electrochim. Acta 134 (2014) 377–383.
[27] T.F. Yi, S.Y. Yang, Y.R. Zhu, M.F. Ye, Y. Xie, R.S. Zhu, Enhanced rate performance of $Li_4Ti_5O_{12}$ anode material by ethanol-assisted hydrothermal synthesis for lithium-ion battery, Ceram. Int. 40 (2014) 9853–9858.
[28] Y. Shi, J. Gao, H.D. Abruña, H.K. Liu, H.J. Li, J.Z. Wang, Y.P. Wu, Rapid synthesis of $Li_4Ti_5O_{12}$/graphene composite with superior rate capability by a microwave-assisted hydrothermal method, Nano Energy 8 (2014) 297–304.
[29] J. Liu, P.J. Lu, S.Q. Liang, J. Liu, W.J. Wang, M. Lei, S.S. Tang, Q. Yang, Ultrathin Li_3VO_4 nanoribbon/graphene sandwich-like nanostructures with ultrahigh lithium ion storage properties, Nano Energy 12 (2015) 709–724.